

See discussions, stats, and author profiles for this publication at: <https://www.researchgate.net/publication/2792108>

# Sphere Tracing: A Geometric Method for the Antialiased Ray Tracing of Implicit Surfaces

Article in *The Visual Computer* · June 1995

DOI: 10.1007/s003710050084 · Source: CiteSeer

---

CITATIONS

336

READS

5,686

1 author:



**John C. Hart**

University of Illinois, Urbana-Champaign

152 PUBLICATIONS 6,548 CITATIONS

SEE PROFILE

Some of the authors of this publication are also working on these related projects:



Fractals [View project](#)



Crops In-Silico [View project](#)

# Sphere Tracing: A Geometric Method for the Antialiased Ray Tracing of Implicit Surfaces\*

John C. Hart

School of EECS

Washington State University

Pullman, WA 99164-2752

(509) 335-2343

(509) 335-3818 (fax)

hart@eecs.wsu.edu

## Abstract

Sphere tracing is a new technique for rendering implicit surfaces using geometric distance. Distance-based models are common in computer-aided geometric design and in the modeling of articulated figures. Given a function returning the distance to an object, sphere tracing marches along the ray toward its first intersection in steps guaranteed not to penetrate the implicit surface.

Sphere tracing is particularly adept at rendering pathological surfaces. Creased and rough implicit surfaces are defined by functions with discontinuous or undefined derivatives. Current root finding techniques such as L-G surfaces and interval analysis require periodic evaluation of the derivative, and their behavior is dependent on the behavior of the derivative. Sphere tracing requires only a bound on the magnitude of the derivative, robustly avoiding problems

---

\*Manuscript, July 1994. Recommended for publication: *The Visual Computer*.

where the derivative jumps or vanishes. This robustness and scope support sphere tracing as an efficient direct visualization system for the design and investigation of new implicit models.

Furthermore, sphere tracing efficiently approximates cone tracing, supporting symbolic-prefiltered antialiasing. Signed distance functions for a variety of primitives and operations are derived and appear independently as appendices, specifically the natural quadrics and torus, superquadrics, Bezier-based generalized cylinders and offset surfaces, constructive solid geometry, pseudonorm and Gaussian blends, taper, twist and hypertexture.

**Keywords:** area sampling, blending, deformation, distance, implicit surface, Lipschitz condition, numerical methods, ray tracing, solid modeling.

## 1 Introduction

Whereas a parametric surface is defined by a function which, given a tuple of parameters, indicates a corresponding location in space, an implicit surface is defined by a function which, given a point in space, indicates whether the point is inside, on or outside the surface.

The most commonly studied form of implicit surfaces are algebraic surfaces, defined implicitly by a polynomial function. For example, the unit sphere is defined by the second degree algebraic implicit equation

$$x^2 + y^2 + z^2 - 1 = 0 \tag{1}$$

as the locus of coordinates whose hypotenuse (squared) is unity.

Alternatively, using a distance metric, one can represent the unit sphere geometrically by the implicit equation

$$\|\mathbf{x}\| - 1 = 0 \tag{2}$$

as the locus of points of unit distance from the origin. Here  $\mathbf{x} = (x, y, z)$  and  $\|(x, y, z)\|$  denotes the Euclidean magnitude  $\sqrt{x^2 + y^2 + z^2}$ . The implicit surface of (2) agrees with that of (1), though their values differ at almost every other point in  $\mathbb{R}^3$ . Specifically, (1) returns *algebraic distance* [Rockwood & Owen, 1987] whereas (2) returns *geometric distance*.

A comparison of geometric versus algebraic representations of quadric surfaces preferred the geometric representation [Goldman, 1983]. The parameters of a geometric representation are coordinate-independent, and are more robust and intuitive than algebraic coefficients. Distance-based functions like (2) are one method for representing implicit surfaces geometrically.

Distance-based models can be found in a variety of areas. *Offset* surfaces have become valuable in computer-aided geometric design for their use of distance to model the physical capabilities of machine cutting tools [Barnhill *et al*, 1992]. *Skeletal* models, which in computer graphics simulate articulated figures such as hands and dinosaurs, are equivalent to offset surfaces. Computer vision's medial-axis transform converts a given shape to its skeletal representation [Ballard & Brown, 1982]. *Generalized cylinders* began as a geometric representation in computer vision [Agin & Binford, 1976] but have also matured into a standard modeling primitive in computer graphics [Bloomenthal, 1989] --- special ray tracing algorithms were developed for their rendering in [van Wijk, 1984; Bronsvoort & Klok, 1985].

## 1.1 Previous Work

Several methods exist for rendering implicit surfaces. Indirect methods polygonize the implicit surface to a given tolerance, allowing the use of existing polygon rendering techniques and hardware for interactive inspection [Wyvill *et al*, 1986; Bloomenthal, 1988]. Although polygonization transforms implicit surfaces into a representation easily rendered and incorporated into graphics systems, polygonizations are typically not guaranteed and may not accurately detect disconnected or detailed sections of the implicit surface. Production ray tracing systems tend to polygonize surfaces, resulting in large time and memory overhead to accurately represent an otherwise simple implicit model.

In an effort to combine speed and accuracy, [Sederberg & Zundel, 1989] developed a direct scan-line method to more accurately render algebraic implicit surfaces at interactive speeds. Ray tracing, on the other hand, is a direct, accurate and elegant method for investigating a much larger variety of implicit surfaces.

Let

$$\mathbf{r}(t) = \mathbf{r}_o + t\mathbf{r}_d \quad (3)$$

parametrically define a ray anchored at  $\mathbf{r}_o$  in the direction of the unit vector  $\mathbf{r}_d$ . Plugging the ray equation  $\mathbf{r} : \mathbb{R} \rightarrow \mathbb{R}^3$  into the function  $f : \mathbb{R}^3 \rightarrow \mathbb{R}$  that defines the implicit surface produces the composite real function  $F : \mathbb{R} \rightarrow \mathbb{R}$  where  $F = f \circ \mathbf{r}$  such that the solutions to

$$F(t) = 0 \quad (4)$$

correspond to ray intersections with the implicit surface. Implicit surface ray-tracing algorithms simply apply one of the multitude of numerical root finding methods to solve (4).

When  $f(\mathbf{x}) = 0$  implicitly defines an algebraic surface, (4) is a polynomial equation. Analytic solutions exist for polynomials of degree four or less, but may not be the best numerical method in certain cases. In this and higher degree cases, solving requires an iterative root finding algorithm. Some algebraic surface renderers have used DesCartes' rule of signs [Hanrahan, 1983], Sturm sequences [van Wijk, 1984], and Laguerre's method [Wyvill & Trotman, 1990], which capitalize on properties of polynomials, and are hence more efficient than general root finders.

One must use a general root finder to render the implicit surface of an arbitrary function. Ideally, this root finder should only need the ability to evaluate the function at any point. However, one can always construct a pathological function that will cause such a "blind" technique to miss one or more roots, by inserting an arbitrarily thin region between samples where the function zips off to zero and back (a point reiterated from [Kalra & Barr, 1989; Von Herzen *et al*, 1990]). Hence, any robust root finder needs more information than simple function evaluation.

The "Hypertexture" system used a brute-force blind ray-marching scheme, using only function evaluation [Perlin & Hoffert, 1989]. Its lack of robustness required fine sampling along the ray, resulting in rendering speeds so slow they demanded parallel implementation. Requiring only function evaluation allowed the design of implicit surfaces without regard to the analytic properties of their defining functions. Freed from such constraints, fractal and hairy surfaces were easily modeled by implicit surfaces whose functions contained procedural elements.

Robust ray intersection requires extra information, which in most cases is produced by the derivative of the function. Current techniques repeatedly subdivide the graph of  $F(t)$  until it is

partitioned into intervals that either do not intersect the  $t$ -axis, corresponding to no ray intersection, or the graph of the derivative  $F'(t)$  does not intersect the  $t$ -axis, corresponding to only one ray intersection. The root within such an interval is refined using Newton's method and *regula falsi*. In the rare case of a multiple root, such as when a ray grazes a surface or intersects coincident surfaces, the root isolation process subdivides the interval surrounding the root to machine precision.

Interval analysis finds ray intersections by defining the function and its derivative on intervals instead of single values. It uses such interval arithmetic operations to bound the values of  $F$  and its derivative  $F'$ . Over an interval, if the bound of  $F$  omits zero, then there is no root. Otherwise if the bound of  $F'$  omits zero, then there is a single root. Otherwise the interval is subdivided at its midpoint [Mitchell, 1990b].

Lipschitz methods are an alternative to interval analysis. (Lipschitz and interval methods are compared in Section 2.3.) As described by Section 2.1, a function is Lipschitz if and only if the magnitude of its derivative remains bounded. The LG-surfaces method imposed the Lipschitz condition on the derivative  $F'$  over an interval, yielding a bound  $G$  on the magnitude of  $F''$ . This bound  $G$  is a speed limit on  $F'$ , meaning that the range of  $F'$  can change only  $G$  times as fast as its domain. If the value of  $F'$  at one of the endpoints of an interval is more than  $G$  times the length of the interval away from zero, then the Lipschitz condition guarantees that the derivative  $F'$  is never zero. The original function  $F$  then contains no roots over the interval if its value at the interval's endpoints have the same sign, or one root if the sign of its endpoints differ [Kalra & Barr, 1989].

## 1.2 Overview

Sphere tracing is a robust technique for ray tracing implicit surfaces. Unlike LG-surfaces or interval analysis, it does not require the ability to evaluate the derivative of the function. Instead, it requires only a bound on the magnitude of the derivative --- that the function be continuous and Lipschitz. Thus, the derivative of the function need not be continuous, nor even defined.

Sphere tracing benefits from this relaxation by using the continuous but non-differentiable minimum and maximum operations for constructive solid geometry instead of the commonly used Roth diagrams [Roth, 1982]. Unlike typical ray tracers, sphere tracing can concentrate on finding

only the first ray intersection of a CSG model, avoiding the expense of finding all ray-component intersections. Defining CSG using minimum and maximum operations also allows sphere tracing to render the results of blending and other geometric operations on CSG models, which is impossible using Roth diagrams.

Sphere tracing also allows the efficient visualization a wider range of implicit surfaces than before possible, including creased, rough and fractal surfaces. Like the slower brute-force rendering approach of the “Hypertexture” system [Perlin & Hoffert, 1989], sphere tracing frees the implicit surface designer from many concerns regarding the analytic behavior of the defining function, fostering more diverse implicit formulations. Moreover, structures in mathematics are often specified as the locus of points that satisfy a particular condition. Sphere tracing visualizes such structures, regardless of smoothness, extent and connectedness, given only a bound on the rate of the condition’s continuous changes over space. Sphere tracing provides a direct and flexible visualization tool for the development of new implicit models.

Sphere tracing approximates cone tracing [Amanatides, 1984] to eliminate aliasing artifacts and simulate soft shadows. Aliasing artifacts are typically reduced by stochastic supersampling, where many randomly-directed rays are cast for each pixel. Supersampling inhibits aliasing by moving the artifacts into higher frequencies, and stochastic sampling disguises the artifacts as uncorrelated noise [Mitchell, 1990a]. Cone tracing, on the other hand, eliminates aliasing by prefiltering the scene, so a single point sample accurately represents the average of its neighborhood. In addition to the better treatment of antialiasing cone tracing provides, implicit surfaces are often defined by very expensive functions, and reducing the number of function evaluations by tracing a single cone per pixel, instead of many rays per pixel, makes antialiasing more efficient.

## 2 Sphere Tracing

Sphere tracing capitalizes on functions that return the distance to their implicit surfaces (Section 2.1) to define a sequence of points (Section 2.2) that converges linearly to the first ray-surface intersection (Section 2.3). Section 2.4 compares Lipschitz methods to interval analysis. Section 2.5

incorporates constructive solid geometry into sphere tracing at the model level. Section 2.6 describes several enhancements to sphere tracing to hasten convergence.

## 2.1 Distance Surfaces

This section defines and discusses functions that measure or bound the geometric distance to their implicit surfaces. Such functions implicitly define *distance surfaces*, as mentioned in [Bloomenthal & Shoemake, 1991]. The appendices derive functions that measure or bound distances for a variety of primitives and operations.

Let the function  $f$  be a continuous mapping  $f : \mathbb{R}^n \rightarrow \mathbb{R}$  that implicitly describes the set  $A \subset \mathbb{R}^n$  as the locus of points

$$A = \{\mathbf{x} : f(\mathbf{x}) \leq 0\}. \quad (5)$$

By continuity,  $f$  is zero on the boundary  $\partial A$  which forms the *implicit surface* of  $f$ . Furthermore,  $f$  is expected to be strictly negative over the interior  $\overset{\circ}{A}$ , which allows the multivalued function image  $f^{-1}(0)$  to concisely represent the implicit surface of  $f$ .

**Definition 1** The point-to-set distance defines the distance from a point  $\mathbf{x} \in \mathbb{R}^3$  to a set  $A \subset \mathbb{R}^3$  as the distance from  $\mathbf{x}$  to the closest point in  $A$ ,

$$d(\mathbf{x}, A) = \min_{\mathbf{y} \in A} \|\mathbf{x} - \mathbf{y}\|. \quad (6)$$

Given a set  $A$ , the point-to-set distance  $d(\mathbf{x}, A)$  implicitly defines  $A$  (from the outside) [Kaplansky, 1977]. Here, we are interested in the converse: *Given an implicit function, what is the point-to-set distance to its surface?*

**Definition 2** A function  $f : \mathbb{R}^3 \rightarrow \mathbb{R}$  is a *signed distance bound* of its implicit surface  $f^{-1}(0)$  if and only if

$$|f(\mathbf{x})| \leq d(\mathbf{x}, f^{-1}(0)). \quad (7)$$

If equality holds for (7), then  $f$  is a *signed distance function*.

Some primitives, such as the sphere, are easily defined with signed distance functions. Finding the distance to other shapes can be quite difficult. Table 1 lists the primitives and operations for which the appendices contain signed distance functions and bounds.

The Lipschitz constant is a useful quantity for deriving signed distance bounds to complex shapes.

**Definition 3** A function  $f : \mathbb{R}^3 \rightarrow \mathbb{R}$  is *Lipschitz* over a domain  $D$  if and only if for all  $\mathbf{x}, \mathbf{y} \in D$ , there exists a positive finite constant  $\lambda$  such that

$$|f(\mathbf{x}) - f(\mathbf{y})| \leq \lambda \|\mathbf{x} - \mathbf{y}\|. \quad (8)$$

The *Lipschitz constant*, denoted  $\text{Lip } f$ , is the minimum  $\lambda$  satisfying (8).

The Lipschitz constant has been used in computer graphics for collision detection [Von Herzen & Barr, 1987] and rendering implicit functions [Kalra & Barr, 1989]. The Lipschitz constant is the tightest possible bound on the magnitude of the derivative of a function.

In practice, Lipschitz constants are typically overestimated by a *Lipschitz bound*, particularly for functions whose components have known Lipschitz constants. For example, the Lipschitz constant of the sum of two functions is at most the sum of their Lipschitz bounds. By the chain rule, the Lipschitz constant of the composition of functions is at most the product of the component function's Lipschitz constants.

One can determine the Lipschitz constant of a continuous function algebraically as the maximum slope of the function. This maximum slope occurs at one of the zeroes of the function's second derivative. Often geometric observations serve the investigator better than algebraic manipulation for determining the Lipschitz constant. For example, notice the simplified algebraic Lipschitz derivations for soft objects in Appendix D or the completely geometric derivation for twisted objects in Appendix E.

The following theorem shows how to turn a Lipschitz function into a signed distance bound, allowing sphere tracing to render any implicit surface defined by a Lipschitz function.

**Theorem 1** *Let  $f$  be Lipschitz with Lipschitz bound  $\lambda \geq \text{Lip } f$ . Then the function  $f/\lambda$  is a signed distance bound of its implicit surface.*

Primitive/Operation	Signed Distance Function	Signed Distance Bound
plane	Appendix A	
sphere	Appendix A	
ellipsoid	[Hart, 1994]	Appendix A & E
cylinder	Appendix A	
cone	Appendix A	
torus	Appendix A	
superquadrics		Appendix B
generalized cylinder	Appendix C	
union	Section 2.5	
intersection		Section 2.5
complement	Section 2.5	
soft objects		Section D
pseudonorm blend	[Rockwood, 1989]	Appendix D
isometry	Appendix E	
uniform scale	Appendix E	
linear transformation		Appendix E
taper		Appendix E
twist		Appendix E
hypertexture		Appendix F
fractals		Appendix F

Table 1: Directory of signed distance functions and bounds.

**Proof:** Given a point  $\mathbf{x}$ , let  $\mathbf{y} \in f^{-1}(0)$  be one of the points such that

$$\|\mathbf{x} - \mathbf{y}\| = d(\mathbf{x}, f^{-1}(0)). \quad (9)$$

Then by (8) and  $f(\mathbf{y}) = 0$  it follows that

$$|f(\mathbf{x})| \leq \lambda d(\mathbf{x}, f^{-1}(0)). \quad (10)$$

Hence,  $\lambda^{-1}f(\mathbf{x})$  is a signed distance bound for any Lipschitz function  $f$ . (Compare Eq. (8) of [Kalra & Barr, 1989]).  $\square$

Using the Lipschitz constant in (10) results in an optimal signed distance bound. A looser Lipschitz bounds causes a poorer distance underestimate, which adversely affect the efficiency of algorithms that use it.

## 2.2 Ray Intersection

One intersects a ray  $\mathbf{r}(t)$  with the implicit surface defined by the signed distance bound  $f(\mathbf{x})$  by finding its least positive root (the *first* root) of  $F(t)$ . This root is the limit point of the sequence defined by the recurrence equation

$$t_{i+1} = t_i + F(t_i) \quad (11)$$

and the initial point  $t_0 = 0$ . The sequence converges if and only if the ray intersects the implicit surface. This sequence forms the kernel of the geometric implicit surface rendering algorithm in Figure 1.

The convergence test  $\epsilon$  is set to the desired precision. The maximum distance  $D$  corresponds to the radius of a viewer-centered yonder clipping sphere, and is necessary to detect non-convergent sequences.

The absolute value of the signed distance function can be considered the radius of a sphere guaranteed not to penetrate any of the implicit surface. This sphere was called an *unbounding* sphere in [Hart *et al*, 1989] (which used a distance bound to implicitly define and visualize 3-D deterministic fractals) because the implicit surface is contained in the closed complement of this sphere. Unlike a bounding volume which surrounds an object, an unbounding volume surrounds

Given signed distance bound  $f$ , ray  $\mathbf{r}(t)$  and maximum ray traversal distance  $D$ .

Initialize  $t = 0$  and  $d = 0$

While  $t < D$

    Let  $d = f(\mathbf{r}(t))$

    If  $d < \epsilon$  then return  $t$  --- *intersection*

    Increment  $t = t + d$

return  $\emptyset$  --- *no intersection*

Figure 1: Pseudocode of the geometric implicit surface rendering algorithm.

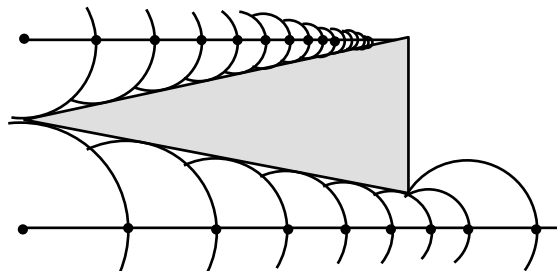


Figure 2: A hit and a miss.

an area of space not containing the object. The name “sphere tracing” arose from the property that ray intersections are determined by sequences of unbounding spheres.

As did [Ricci, 1974], sphere tracing uses the minimum and maximum functions for constructive solid geometry. These operations crease the implicit surface locally, such that the defining function remains continuous in value, but not in derivative. Derivative discontinuity can cause problems with root finders, which must find all roots of the function and resolve the CSG operation using a Roth diagram [Roth, 1982]. Sphere tracing operates independent of the derivative, given its bound, and need converge only to the first root, even for CSG models.

### 2.3 Analysis

Root refinement methods, such as Newton’s method, converge quadratically to simple roots (where the ray penetrates the surface), and linearly to multiple roots (where the ray grazes the surface) [Gerald & Wheatley, 1989]. Root isolation methods which divide and conquer, such as LG-surfaces [Kalra & Barr, 1989] and interval analysis [Mitchell, 1990b], converge linearly since the width of the intervals are reduced by a factor of one-half at each iteration. Root isolation methods are allowed to converge only in the event of a multiple root, otherwise they pass control to a faster root refinement method the moment they find a monotonic region straddling the  $t$ -axis.

**Theorem 2** *Given a function  $F : \mathbb{R} \rightarrow \mathbb{R}$  with Lipschitz bound  $\lambda \geq \text{Lip } F$ , and an initial point  $t_0$ , sphere tracing converges linearly to the smallest root greater than  $t_0$ .*

The sphere-tracing sequence can be written

$$t_{i+1} = g(t_i) = t_i + \frac{|F(t_i)|}{\lambda}. \quad (12)$$

In this form, the similarities of (12) to Newton’s method are more visible. Let  $r$  be the smallest root greater than the initial point  $t_0$ . Since  $F(r) = 0$  then  $g(r) = r$ , and at any non-root  $|F|/\lambda$  is positive. Hence (12) converges to the first root.

Without loss of generality,  $F$  is assumed to be non-negative in the region of interest, which eliminates the need for the absolute value. The Taylor expansion of  $F(t_i)$  about the root  $r$  is

$$g(t_i) = g(r) + (t_i - r)g'(r) + \frac{(t_i - r)^2}{2}g''(\tau) \quad (13)$$

for some  $\tau \in [t_i, r]$  and  $g'(r) = 1 + F'(y)/\lambda$ . The error term becomes

$$e_{i+1} = t_{i+1} - r = g(t_i) - g(r) = g'(r)e_i + \text{higher order terms} \quad (14)$$

Since  $g'(r)$  is constant in the iteration, (12) converges linearly to  $y$ .  $\square$

**Corollary 2.1** *Sphere tracing converges quadratically if and only if the function is steepest at its first root.*

In the event  $F'(r) = -\lambda$ , the linear term of the error (13) drops out, leaving the quadratic and higher order terms.  $\square$

## 2.4 Lipschitz Methods vs. Interval Analysis

Subdivision-based Lipschitz methods [Von Herzen & Barr, 1987; Von Herzen *et al*, 1990; Kalra & Barr, 1989] have been replaced by similar but more flexible interval methods [Mitchell, 1990b; Snyder, 1992]. The use of interval arithmetic and automatic differentiation in the definition of a function [Mitchell & Hanrahan, 1992] isolate root finding information from the user, whereas the use of Lipschitz bounds generally require the user to understand the function well enough to know how tightly it contracts points. However, both methods involve similar operations.

Let  $f : \mathbb{R} \rightarrow \mathbb{R}$  be a function over an interval  $X \subset \mathbb{R}$ . Defining  $f$  with interval arithmetic operations results in an interval value  $[a, b] = f(X)$  bounding the values of  $f$  over  $X$ . (We assume the first value  $a$  is no greater than the second value  $b$  for all intervals.) Moreover, the interval  $[a', b'] = f'(X)$  bounds the values of the derivative  $f'$  over  $X$ . A Lipschitz bound of  $f$  over the domain  $X$  is given by

$$\text{Lip}_X f \leq \max(-a', b') \quad (15)$$

whereas the interval  $[-\text{Lip}_X f, \text{Lip}_X f]$  bounds all possible values of  $f'$  over  $X$ .

The rules of interval arithmetic are similar to the addition and composition rules of Lipschitz bounds. They are designed for a worst case that may not actually happen over a given domain. Interval arithmetic abstracts the bounding of a function's values, such that the user need not check its results. Interval arithmetic bounds functions from the bottom up, by bounding the function's components and then their compositions.

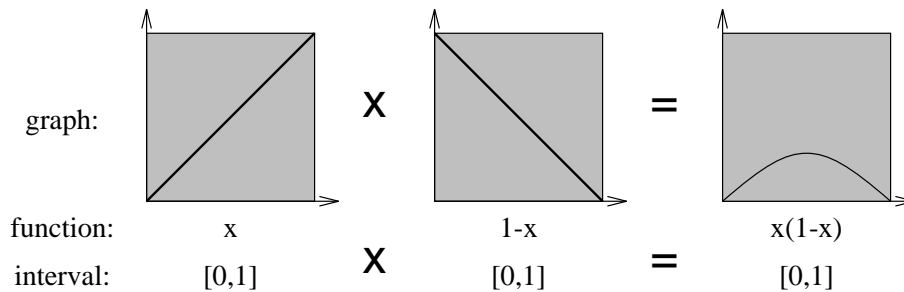


Figure 3: Interval arithmetic resulting in a loose bound of a parabola.

For example, Figure 3 illustrates a parabola defined by the function  $f(x) = x(1 - x)$  created as the product of  $x$  and  $1 - x$ . The interval bound of both monotonic component functions is defined optimally as  $[0, 1]$ . Their interval product  $[0, 1] \times [0, 1] = [0, 1]$  is four times larger than the optimal bound  $[0, \frac{1}{4}]$  of the product  $x(1 - x)$ . Moreover, treating  $x(1 - x)$  as  $x + -(x \times x)$  yields an even worse interval bound of  $[-1, 1]$ .

Although Lipschitz bounds can be found using rules similar to interval arithmetic, they are often designed from the top down instead, through a holistic understanding of the function and its metric effects. This process can yield a tighter, often optimal Lipschitz bound on the function than is possible by simple interval arithmetic of its components.

Sphere tracing differs from previous Lipschitz-based methods in computer graphics in that it is not based on binary subdivision. An interval version of sphere tracing could use (15) to define a (local) Lipschitz bound, although any creases in the domain would yield a useless (for sphere tracing) derivative interval of  $[-\infty, \infty]$ , as prescribed in [Mitchell, 1990b].

## 2.5 Constructive Solid Geometry

Following [Ricci, 1974], the minimum and maximum operations on functions results in union and intersection operations on their implicit surfaces. In the following equations, let  $f_A, f_B$  be signed distance functions of sets  $A$  and  $B$  respectively. If  $f_A$  or  $f_B$  is a signed distance bound, then the resulting CSG implicit function will be also be a bound.

The distance to the union of  $A$  and  $B$  is the distance to the closer of the two

$$d(\mathbf{x}, A \cup B) = \min f_A(\mathbf{x}), f_B(\mathbf{x}). \quad (16)$$

Similarly, the distance to a list of objects is the smallest of the distances to each of the component objects.

The distance to the complement of  $A$  takes advantage of the signed nature of the distance function

$$d(\mathbf{x}, \mathbb{R}^3 \setminus A) = -f_A(\mathbf{x}). \quad (17)$$

Although DeMorgan's theorem defines intersection as the complement of the union of complements, the minimum operators used in the union are not complemented properly. Instead, the distance to the intersection is bound by the distance to the farthest component.

**Theorem 3** *The distance from a point  $\mathbf{x}$  to the intersection of two implicit surfaces  $A = f_A^{-1}(0)$  and  $B = f_B^{-1}(0)$  defined by signed distance bounds  $f_A, f_B$  is bounded by*

$$d(\mathbf{x}, A \cap B) \geq \max f_A(\mathbf{x}), f_B(\mathbf{x}). \quad (18)$$

**Proof:** By parts, as illustrated on a sample intersection in Figure 4.

Case I:  $\mathbf{x} \in A \cap B$ . Both  $f_A$  and  $f_B$  are negative, and the larger of the two indicates the (negative) distance to the closest edge of the intersection.

Case II:  $\mathbf{x} \in A, \mathbf{x} \notin B$ . The function  $f_A$  is negative whereas  $f_B$  is positive, hence the greater of the two. The closest point on  $B$  to  $\mathbf{x}$  may not be in the intersection, but there cannot be any point in the intersection closer.

Case III:  $\mathbf{x} \notin A, \mathbf{x} \in B$ . Symmetric with Case II.

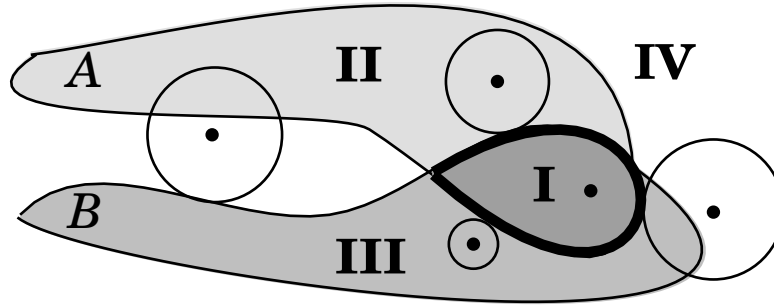


Figure 4: Sample points illustrated a bound on the distance to the intersection between two sets.

Case IV:  $x \notin A \cup B$ . As before, the closest point in the intersection  $A \cap B$  can be no closer than the farther of the closest point in  $A$  and the closest point in  $B$ .  $\square$

From its definition, set subtraction  $A - B$  may be simulated as  $A \cap (\mathbb{R}^3 \setminus B)$ , though yielding only a signed distance bound due to the intersection operator.

The union and intersection operators are demonstrated in Figure 10 in Section 4.2.

## 2.6 Enhancements

The following enhancements increase the efficiency of sphere tracing by reducing unnecessary distance computations, which can be quite expensive and even iterative in some cases. The enhancements are evaluated and analyzed empirically in Section 4.3.

### 2.6.1 Image Coherence

An algorithm similar to sphere tracing has been developed for rendering discrete volumetric data using the 3-D *distance transform* [Zuiderveld *et al.*, 1992]. The distance transform takes a binary “filled/unfilled” voxel array to a numerical voxel array such that each voxel contains the distance to the closest “filled” voxel, under a given metric. We have also extended the concept of Lipschitz constants to volume rendering [Stander & Hart, 1994], trading the distance transform for an octree of local Lipschitz constants as in [Kalra & Barr, 1989], allowing distance-based accelerated volume rendering of arbitrary isovalued surfaces while eliminating the need to recompute the preprocessed data structure for each change in the threshold.

One enhancement in [Zuiderveld *et al*, 1992] kept track of the smallest distance encountered by a ray that misses the object. Under an orthogonal projection, this smallest distance defines the radius of a disk of guaranteed empty pixels surrounding the sample point. Under a perspective projection, the minimum *projected* distance must be computed (requiring ray-sphere intersection), and this enhancement becomes less efficient. Initial tests have shown this enhancement to degrade performance in the perspective case for typical implicit surfaces.

## 2.6.2 Bounding Volumes

Bounding volumes are a useful mechanism to cull processing of intricate geometries which are irrelevant to the current task. Beyond their typical benefit of avoiding the casting of rays that miss an object, they also help sphere tracing avoid distance computations for objects farther away than others. The overhead of quick bounding-volume distance checks is, in most cases, a small price to pay for the benefit of avoiding many expensive but useless distance computations.

First, the distances to each bounding volume in a union or collection of objects is computed. Then in order of increasing bounding volume distance, the distance to the contents of each bounding volume is computed until a content's distance is less than the smallest bounding volume distance. This distance is then the point-to-set distance to the collection of objects. This process is sketched in Figure 5.

A Lagrange multiplier method for finding the bounding parallelepiped of an implicit surface appears in [Kay & Kajiya, 1986]. The signed distance bound has properties which might yield an alternative implicit surface bounding volume algorithm, but this topic is left for further research.

## 2.6.3 The Triangle Inequality

The triangle inequality,

$$\|\mathbf{a} - \mathbf{c}\| \leq \|\mathbf{a} - \mathbf{b}\| + \|\mathbf{b} - \mathbf{c}\| \quad \forall \mathbf{a}, \mathbf{b}, \mathbf{c} \in \mathbb{R}^3, \quad (19)$$

is part of the definition of any metric. It can also help eliminate unnecessary distance computations for collections of objects. When computing the shortest distance between a point and a collection

Make a heap  $D$  of bounding volume distances to each object.

Initialize  $d = \infty$ .

Repeat

    Let  $d$  be the lesser of  $d$  or the distance to the contents of the bounding volume at the top of the heap.

    Remove the top of the heap and re-heap.

    Let  $d_h$  be the distance to the bounding volume now at the top of the heap.

Until  $d < d_h$  or the heap is empty.

return  $d$ .

Figure 5: An efficient algorithm for finding the closest object of a collection using bounding volumes.

of objects, one need not compute the distance to objects whose last distance evaluation minus the distance traversed along the ray since that last evaluation is still larger than the distance to the currently closest object. The triangle inequality enhancement algorithm is outlined in Figure 6.

#### **2.6.4 Octree Partitioning**

Eliminating empty space certainly aids rendering efficiency, but the major benefit of partitioning is that it allows the imposition of local bounds on the Lipschitz constants yielding tighter signed distance bounds. Octree partitioning has been used in the polygonization [Bloomenthal, 1989] and ray tracing [Kalra & Barr, 1989] of implicit surfaces. Sphere tracing reaps the same benefits from spatial partitioning as did the root finding method in [Kalra & Barr, 1989], which used the Lipschitz constant to cull octree nodes guaranteed not to intersect the implicit surface.

Ray intersection with an implicit surface defined by a signed distance bound is penalized by the section of the domain where the gradient magnitude is greatest. Chopping an object into the union of smaller chunks allows each chunk to be treated individually, penalized only by the largest gradient within its bounds. Since the partitioning algorithm in [Kalra & Barr, 1989] required only a bound on the Lipschitz constant of the function, the use of this octree in no way restricts the domain of functions available for sphere tracing.

Octree partitioning further enhances sphere tracing of unions and lists by optionally storing an index to the object closest to the cell. An object is closest to an octree cell if and only if it is the closest object to every point in the cell. Under this definition, some cells may not have a closest object. By the triangle inequality (19), an object is closest to a cell if the distance from the cell's centroid to the object, plus the distance from the centroid to the cell corner, is still less than the distance from the centroid to any other object.

#### **2.6.5 Convexity**

Convexity can be defined in any number of ways. For example, metric topology [Kaplansky, 1977] defines a set in a complete metric space as convex if and only if for any two distinct points in the set, there exists a third distinct point whose distance from the first two points sums to their distance

Given ray  $\mathbf{r}(t)$ , maximum distance  $D$  and a collection of objects  $O$ .

Initialize  $d_{\text{last}} = 0$  and  $t = 0$ .

For each object  $o \in O$  initialize  $o_d = 0$ .

Until  $d_{\text{min}} < \epsilon$  or  $t > D$ .

For each object  $o \in O$ .

If  $o_d - d_{\text{last}} > d_{\text{min}}$  then

Update  $o_d = o_d - d_{\text{last}}$ .

Otherwise

Let  $d = d(\mathbf{r}(t), o)$ .

Reset  $o_d = d$ .

Update  $d_{\text{min}} = \min(d_{\text{min}}, d)$ .

End if.

Let  $d_{\text{last}} = d_{\text{min}}$ .

End for.

Update  $t = t + d_{\text{min}}$ .

End until.

Figure 6: Triangle inequality algorithm for avoiding unnecessary distance computations.

from each other. The coordinate space  $\mathbb{R}^3$  allows the more familiar definition of convexity.

**Definition 4** [Farin, 1990] A set  $A \subset \mathbb{R}^3$  is *convex* if and only if the line segment

$$\text{lerp}(\mathbf{x}, \mathbf{y}) = s\mathbf{x} + (1 - s)\mathbf{y}, \quad \forall s \in [0, 1] \quad (20)$$

connecting the two endpoints  $\mathbf{x}, \mathbf{y} \in A$  is a subset of  $A$ .

Knowing that an object is convex can make sphere tracing more efficient by increasing the step size along the ray.

**Theorem 4** Let  $A \subset \mathbb{R}^3$  be a convex set defined implicitly by the signed distance function  $f$ . Then given a unit vector  $\mathbf{v} \in \mathbb{R}^3$  the line segment

$$\text{lerp}\left(\mathbf{x}, \frac{f(\mathbf{x})}{-\mathbf{v} \cdot \nabla f(\mathbf{x})}\mathbf{v}\right) \quad (21)$$

does not intersect  $A$  except possibly at its second endpoint.

**Proof:** The gradient of a signed distance function  $\nabla f$  has the following properties on the complement of a convex set  $\mathbb{R}^3 \setminus A$ : (1) it is continuous; (2) its magnitude is one (the change in the function equals the change in the distance); and (3) its direction points directly away from the closest point on the implicit surface. Hence, for any  $\mathbf{x} \in \mathbb{R}^3 \setminus A$  we know the closest point in  $A$ , and its surface normal points toward  $\mathbf{x}$ . Since  $A$  is convex, it cannot penetrate the tangent plane to  $\mathbf{x}$ .

The intersection of a ray anchored at  $\mathbf{x}$  and direction  $\mathbf{v}$  with the tangent plane normal to the vector  $\nabla f(\mathbf{x})$  a distance of  $f(\mathbf{x})$  from  $\mathbf{x}$  is given by the second endpoint of (21).  $\square$

**Corollary 4.1** If  $\nabla f(\mathbf{x}) \cdot \mathbf{v} \geq 0$  then the ray anchored at  $\mathbf{x}$  and direction  $\mathbf{v}$  does not intersect the implicit surface of  $f$ .

Theorem 4 allows sphere tracing to make larger steps toward convex objects, and Corollary 4.1 allows sphere tracing to avoid computing the distance to convex objects it has stepped beyond. The convexity enhancement likely causes sphere tracing to converge quadratically, because of its similarity to Newton's method, which also converges quadratically.

Bounding volumes are usually convex, and combining these two techniques can further reduce the computation of unnecessary distances.

Knowledge of convexity becomes a necessity for rendering scenes with a horizon line. Consider a ground plane and a ray parallel to it. Sphere tracing will step along this ray at fixed intervals looking for an intersection that never happens. Corollary 4.1 avoids this situation whereas Theorem 4 hastens convergence of rays nearly parallel to the ground plane.

### 3 Antialiasing

Tracing cones instead of rays resulted in an area-sampling antialiasing method in [Amanatides, 1984]. Cone tracing computed the intersection of cones with spheres, planes and polygons to symbolically prefilter an image, eliminating the aliasing artifacts that result from point sampling. Sphere tracing is easily coerced into detecting and approximating cone intersections with any implicit surface defined by a signed distance function. One must still implement the details of the cone tracing algorithm to determine the shape of the cones as they bounce around a scene, but may rely on unbounding spheres to increase the efficiency of determining cone intersections. Moreover, sphere tracing only enhances the detection of cone intersections at silhouette edges, and is of no help in the other forms of aliasing cone tracing also fixes, such as texture aliasing.

At some point along a grazing ray, the sequence of unbounding spheres shrinks, falling within the bounds of the cone, then enlarges, escaping the bounds of the cone. This poses the problem of “choosing a representative” [Amanatides, 1984] --- a location to take a sample to approximate the shading of the cone’s intersection with the surface.

A cover is a pixel-radius offset bounding an implicit surface on the inside and outside such that a ray-cover intersection indicates a cone-object intersection [Thomas *et al*, 1989]. Given an implicit surface defined by the signed distance function  $f(\mathbf{x})$ , its outer cover is the global offset surface implicitly defined by  $f(\mathbf{x}) - r_p$  and its inner cover is the global offset surface implicitly defined by  $f(\mathbf{x}) + r_p$ , where  $r_p$  is the radius of a pixel (one-half of the diameter of a pixel [Hart & DeFanti, 1991]). In other words, the outer cover is the surface  $f^{-1}(r_p)$  and the inner cover is the

surface  $f^{-1}(r_p)$ . Instead of sphere tracing the implicit surface of  $f(\mathbf{x})$ , the antialiasing algorithm sphere traces the inner cover --- the implicit surface of  $f(\mathbf{x}) + r_p$ .

The development of covers proposes the most representative choice for silhouette antialiasing would be the point along the section of the ray closest to the surface. Hence, of the unbounding spheres inside the cone, the center of the smallest sphere (with respect to pixel size) becomes the representative sample. Though this sample is off the implicit surface, one assumes a reasonable level of continuity in the gradient of the distance function to define a usable surface normal. The sequence along the ray of unbounding spheres are related to a cone as shown in Figure 7.

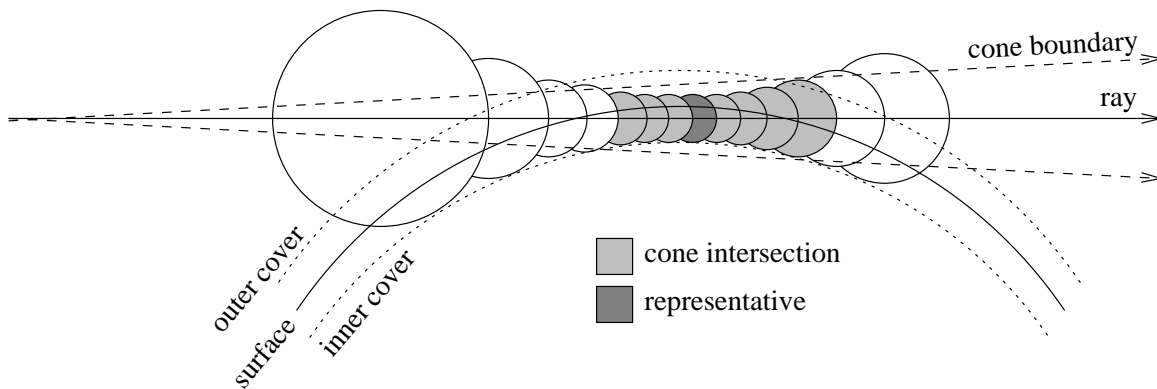


Figure 7: Sphere tracing approximates cone intersection. The ray intersects the original surface but misses its inner cover. This cone intersection will account for more than half of the pixel's illumination.

For smooth implicit surfaces, one may assume local planarity. Hence the implicit surface is assumed to cover the cross section of the cone with a straight edge of the given distance from the cone's center. The amount of influence this shaded point has, with respect to the points the ray intersects further on, depends on the signed distance function evaluated at the representative  $f(\mathbf{x})$  (the radius of the closest unbounding sphere) to the implicit surface. The fraction of coverage of a disk of radius  $r_p$  by an intersecting half-plane of signed distance  $f(\mathbf{x})$  from its center is given by

$$\alpha = \frac{1}{2} - \frac{f(\mathbf{x})\sqrt{r_p^2 - f(\mathbf{x})^2}}{\pi r_p^2} - \frac{1}{\pi} \arcsin \frac{f(\mathbf{x})}{r_p} \quad (22)$$

and is derived in [Thompson, 1990]. Ray traversal proceeds in steps of  $f(\mathbf{x}) + r_p$  (which may take it through the surface). The percentage of coverage  $\alpha$  represents the cone intersection of the grazing

ray. It is treated as an opacity and is accumulated and used to blend the shading of the current representative  $x$  with the shading resulting from further near misses and intersections, using the standard rules of image compositing [Porter & Duff, 1984].

For intersection edges, one must keep track of all signed distance functions whose unbounding spheres fit within the bounds of the cone. Upon ray intersection approximation, the signed distance functions of each of the intersecting surfaces provide the proportions for the proper combination of their shading properties. The representative for intersection is the last point of the ray traversal sequence, the point that satisfies the convergence test.

Often the signed distance function is too expensive to compute efficiently and a signed distance bound is used. A bound may return unbounding spheres whose radii prematurely shrink below the radius of a pixel, resulting in incorrect cone intersections. In this case, a separate distance approximation may be useful. For example, [Pratt, 1987; Taubin, 1994] estimate the distance to the implicit surface of  $f$  with the first order approximation  $f/||\nabla f||$ . In general, this approximation is not necessarily a distance bound. Lemma 1 of [Taubin, 1994] asserts that this approximation is asymptotic to geometric distance as one approaches the surface. Cone intersections can hence be more accurately determined by this approximation than by the signed distance bound.

For texture aliasing, cone tracing filtered the texture based on the radius of the cone at intersection. Since cone tracing is maintained within the unbounding-sphere ray-intersection scheme, textures can be likewise antialiased within this rendering system.

## 4 Results

Sphere tracing simplifies the implementation of an implicit surface ray tracer, and runs at speeds comparable to other implicit surface rendering algorithms.

### 4.1 Implementation

Sphere tracing has been implemented in a rendering system called **zeno**. Inclusion of an implicit surface into **zeno** requires the definition of two functions: a signed distance function for ray

intersection, and a surface normal function for shading.

A new primitive or operation can be incorporated into **zeno** with no more than a distance bound. The negative part of the signed distance bound is only necessary for some constructive solid geometry and blending operations, and is not needed for the visualization of functions that are zero-valued inside the implicit surface. The surface normal function can be avoided by using a general six-sample numerical gradient approximation of the distance bound gradient. Since most of the time is spent on ray intersection, the inefficient numerical gradient approximation has a negligible impact on rendering performance.

The simplicity with which implicit surfaces are incorporated in **zeno** makes it useful for visualization of mathematical tasks and investigation of new implicit surfaces. For example, a homotopy that removes a  $720^\circ$  twist from a ribbon without moving either end formed the basis for the animated short “Air on the Dirac Strings” [Sandin *et al*, 1993], for which **zeno** rendered a segment. This homotopy is based heavily on interpolated quaternion rotations and was easily incorporated into **zeno** as a domain transformation after a quick search and analysis of the most extreme deformation in the homotopy [Hart *et al*, 1993].

## 4.2 Exhibition

The three tori in Figure 8 are combined using the superelliptic blend described in Appendix D.2. The tori all are of major radius one, and minor radius one-tenth. The blue-green blend is quadratic extending along the tori a radius of 0.5 from their intersection. The red-green blend also has radius 0.5 but is degree eight. The red-blue blend is also degree eight but has a radius of only 0.2.

Sphere tracing rendered Figure 8 (left) in 12:47 at a resolution of only  $256 \times 256$  using prefiltering to avoid the severe aliasing that ordinarily accompany such low sampling rates. Experiments on the difference of execution using point sampling and area sampling show that the increased execution time due to area sampling is negligible.

Although the superelliptic blend is implemented in **zeno** as a signed distance bound, it returns an underestimated distance of no less than 70% of the actual distance which adequately indicated cone intersections, as the enlargement demonstrates in Figure 8 (upper right).

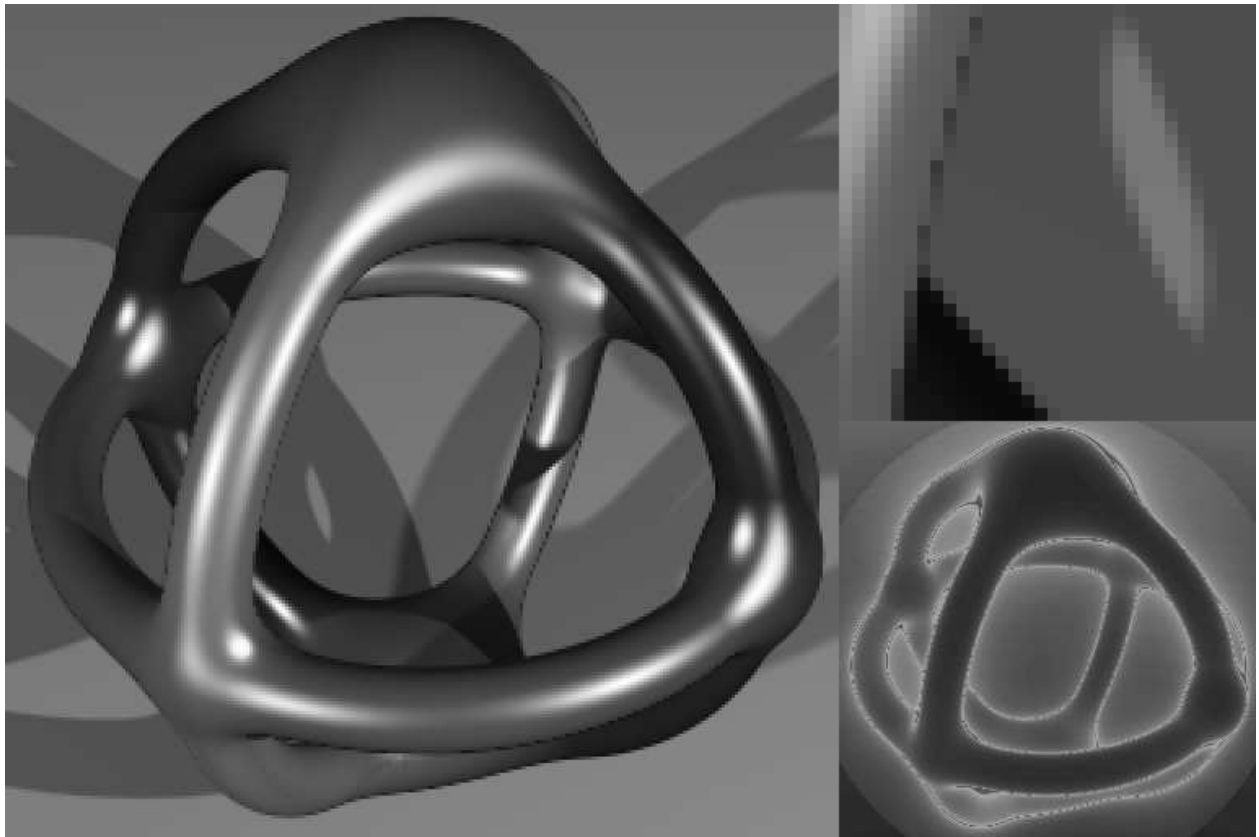


Figure 8: Three blends of tori (left), blowup (upper right) and work image (lower right).

The work image in Figure 8 (lower right) shows that sphere tracing concentrates on silhouette edges. Blue areas converge from 10 iterations, green around 50 and red over 100.

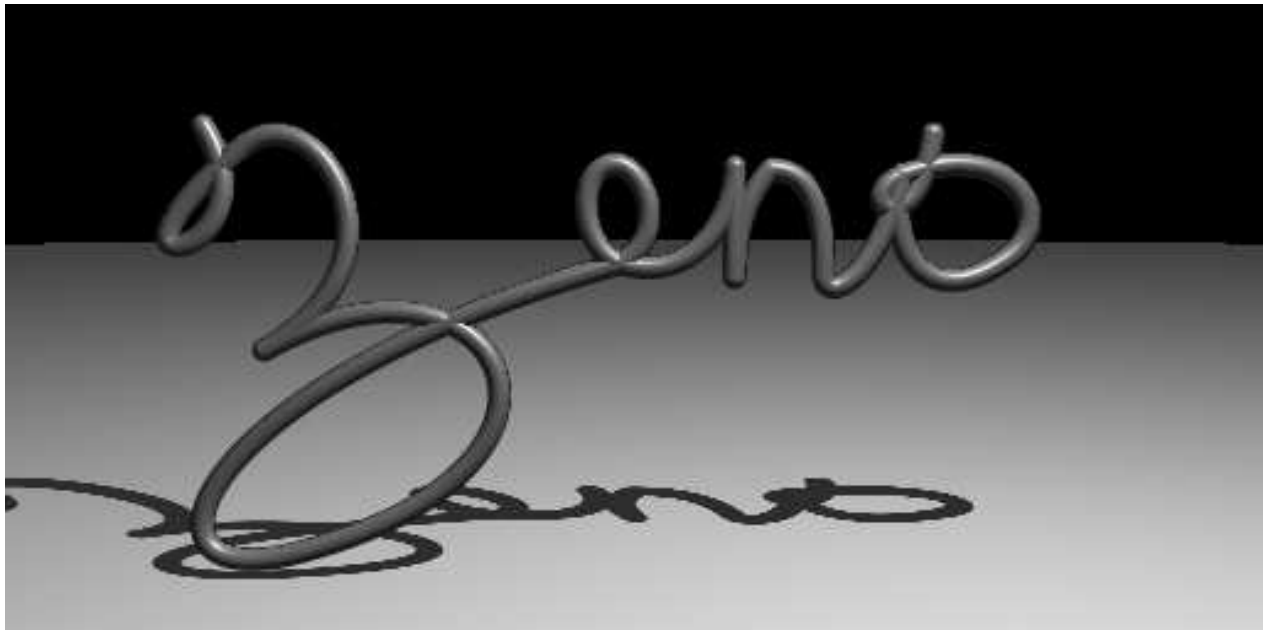


Figure 9: A logo for zeno.

Figure 9 demonstrates a generalized cylinder, from Appendix C, whose skeleton consists of a space curve modeled with 14 Bezier control polygons. Sphere tracing can render this scene in as fast as 5:30 using bounding spheres to eliminate unnecessary distance computations. The curved horizon is an artifact of the yonder clipping sphere of radius 1,000 used to terminate ray stepping.

Figure 10 demonstrates the robustness of sphere tracing on creased surfaces. Both images were rendered with prefiltering at a resolution of  $512 \times 512$ , and in 16:48 for the cylinders, 12:36 for the cube.

The creases were created as CSG unions and intersections, defined implicitly by the continuous but non-differentiable minimum and maximum operations from Section 2.5. The resulting edge was then merged into a third object using the pseudonorm blend from Appendix D.2. Such creased surfaces appear periodically in a variety of shapes, particularly in the modeling of biological forms.

Figure 11 illustrates the ‘‘noise’’ range deformation described in Appendix F. The left image uses a single octave of noise, whereas the next two use six octaves, whose amplitude was scaled

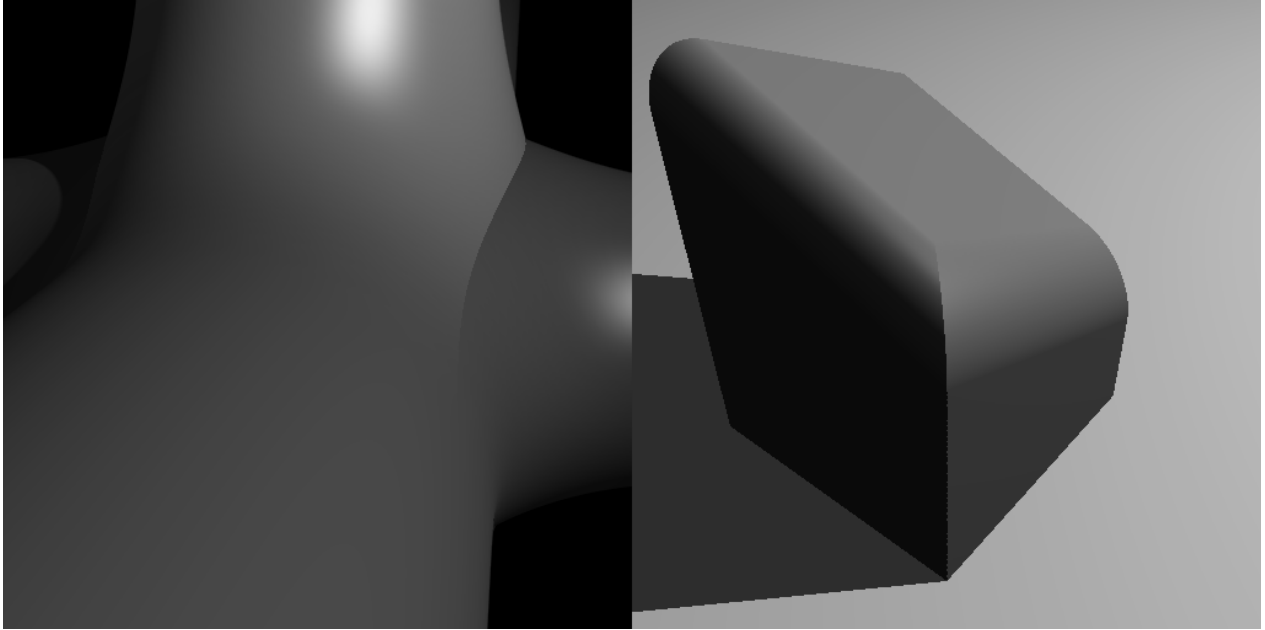


Figure 10: Creases created by blended edges.

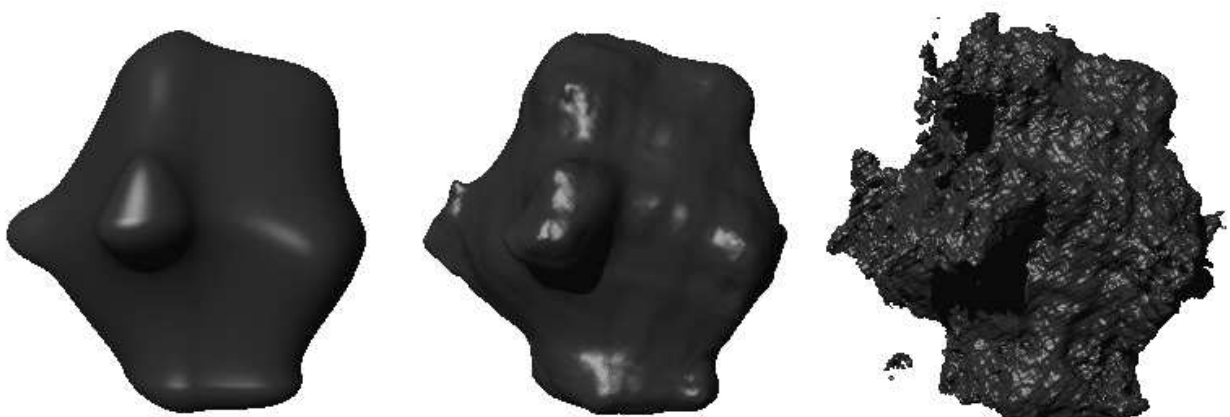


Figure 11: “Lava” (left) modeled as a sphere deformed by the noise function. “Muscle” (center) modeled with Brownian  $1/f^2$  noise. “Rock” (right) modeled with fractional Brownian  $1/f$  noise.

by  $1/f^2$  and  $1/f$ , respectively, yielding a muscle texture and a rocky surface. The three images were each rendered at a resolution of  $256 \times 256$  in (from left to right) approximately five minutes, half-an-hour, and two hours. The high variation of distance estimates prohibited prefiltering the results of the noise function.

### 4.3 Analysis

Sphere tracing convergence is entirely linear whereas other general root finders, such as interval analysis, have a linearly-convergent root isolation phase followed by a quadratically-convergent root refinement stage. Work images, such as Figure 8 (lower right), show that ray intersection is most costly at silhouette edges. When sphere tracing these edges, the distance to the surface is only a fraction of the distance to the ray intersection which slows convergence. For other methods like interval analysis, silhouettes are double roots (that prevent root refinement) and their neighborhoods consist of closely-spaced pairs of roots. Such root pairs are costly for midpoint subdivision root refinement methods to separate since the distance between the two roots can be several orders of magnitude smaller than the initial interval.

The convexity enhancement hastened convergence by 31% as shown in Table 2. With more primitives, this same table shows the triangle inequality enhancement to more than double the convergence rate, and when combined with convexity, enhances ordinary sphere tracing by 60%.

Table 2 also compares various enhanced rendering times for the **zeno** logo. The fact that all 14 Bezier curves were nearly equidistant from the eye prevented the triangle inequality from significantly reducing unnecessary distance evaluations until sphere tracing had traversed much of each ray.

Figure 12 reveals the distribution of step sizes used in sphere tracing a ball. This histogram counted only the distance evaluations used to intersect primary (eye) rays.

Unimproved sphere tracing is evenly distributed, with a small hump in the middle. An octree replaces the increased distance computation in this humped area with octree parsing overhead, (which this histogram does not measure). Echoes of the octree bounds cause the oscillations at the high end of its spectrum, whereas the low end adheres to the unenhanced performance.

scene	execution time	relative time	enhancement
single sphere	2:00	100%	none
	1:23	69%	convexity
9 spheres/plane	2:53	100%	none
	1:42	59%	convexity
	1:19	46%	triangle inequality
	1:10	40%	both
zeno logo	26:29	100%	none
	19:23	73%	triangle inequality
	5:28	21%	bounding spheres
“Lava”	4:37	1	(single noise)
“Muscle”	33:52	7.3	( $1/f^2$ noise)
“Rock”	2:06:56	27.5	( $1/f$ noise)

Table 2: Comparison of execution times for enhanced sphere tracing of various scenes.

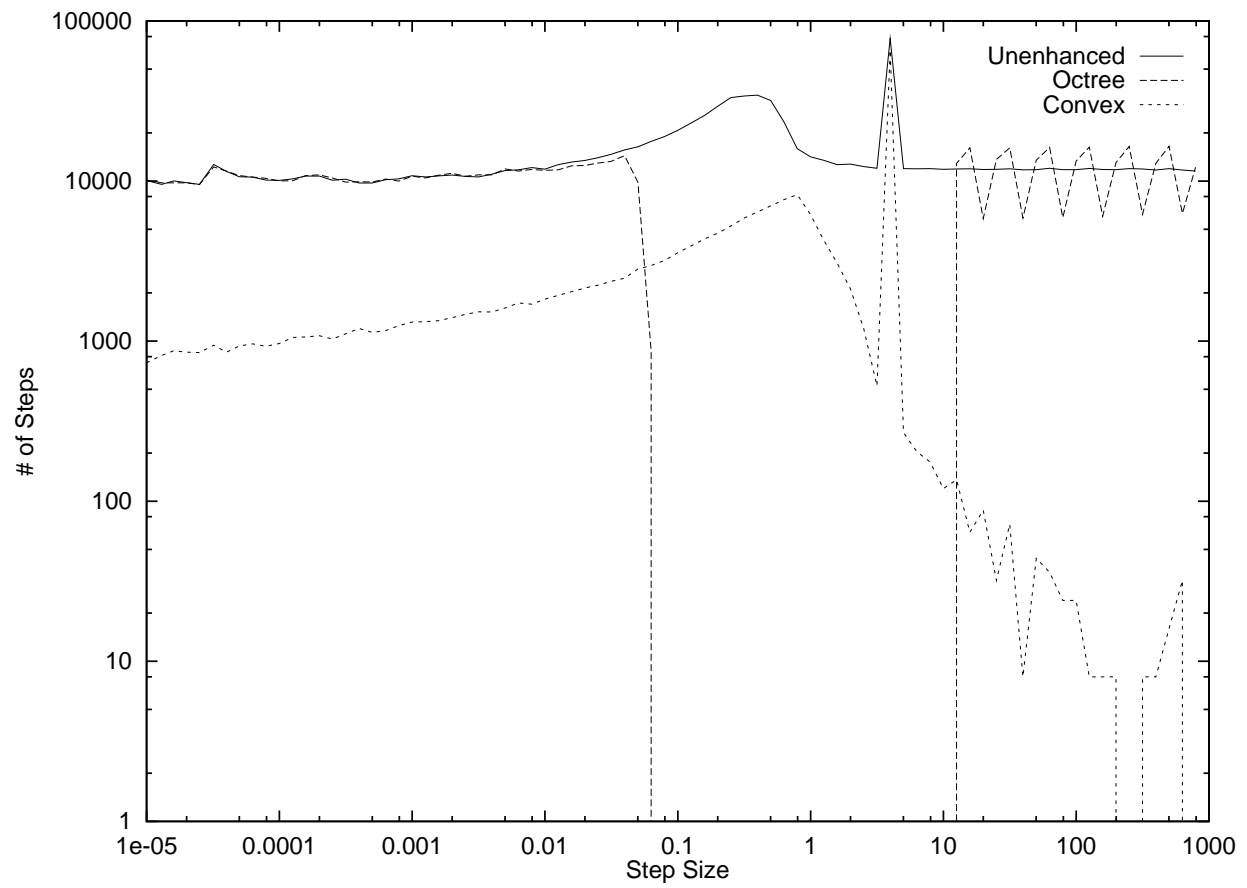


Figure 12: Histogram of step sizes for sphere tracing a ball.

Experiments on simple scenes failed to demonstrate any increased performance from the octree enhancement, although more complicated scenes are likely to benefit from its use.

The convex histogram demonstrates the power of this enhancement. Its slope on the left confirms the expectation from Section 2.6.5 that it provides sphere tracing a faster order of convergence. The right side of this histogram is significantly reduced, due to the cessation of stepping after moving beyond the sphere.

The spike in the unenhanced and convex graphs indicates the distance from the eye to the ball, which is the first step taken by every ray emanating from the eye-point. One can remove these spikes from the graph by measuring this distance once and refer to it as the first step for rays emanating from the eye-point, and likewise for the light sources. This “head start” barely improved performance in experiments.

Similar histograms in [Zuiderveld *et al*, 1992] measured performance logarithmically in the number of steps but linearly in step size. As a result, their graphs were more logarithmically shaped than Figure 12.

The accuracy of the distance estimate is directly proportionate to the rate of convergence. Experiments on a sphere show that half the distance doubles the number of steps. The step-size histograms in Figure 13 reveals the effects of distance underestimation.

The relationship between distance accuracy and sphere tracing performance suggests that in certain cases a slower signed distance function may perform better than a fast distance underestimate. For example, consider the distance to an ellipsoid with major axes of radius 100, 100 and 1 modeled as a non-uniform scale transformation of the unit sphere. Section E yields a signed distance bound which returns at best the distance to the ellipsoid, and at worst 1% of the distance, in closed form, whereas [Hart, 1994] yields a signed distance function which returns the exact distance at the expense of several Newton iterations. In this case, the signed distance function would likely result in better performance.

Finally, the Lipschitz constants of the noise functions are 3 for single noise, 6 for  $1/f^2$  noise and 18 for  $1/f$  noise (six octaves). The timings in Table 2 corresponding to the images in Figure 11 show that the  $1/f^2$ -noise rendering time was actually 7.3 times (instead of the expected value of

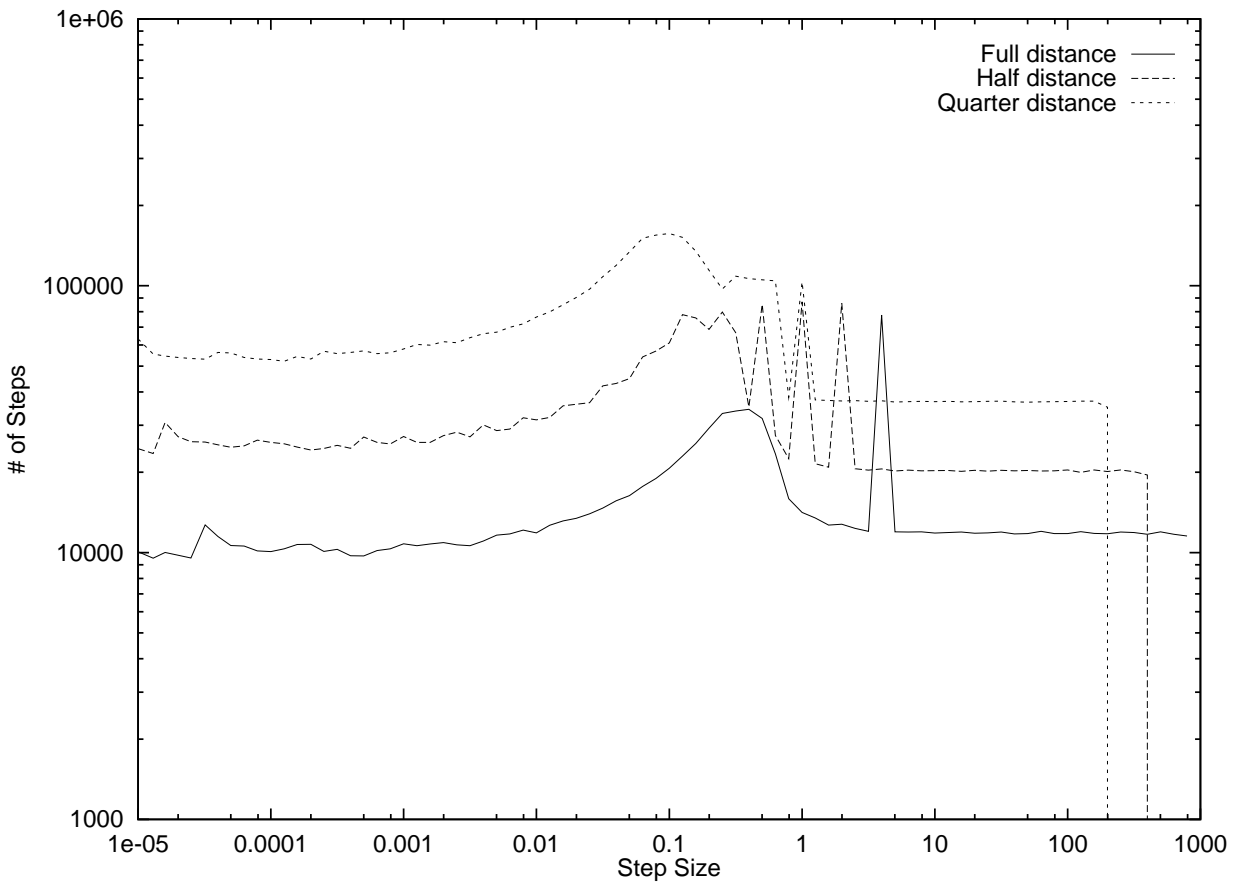


Figure 13: Halving step sizes doubles convergence time.

twice) the single noise time. The likely reason is that the  $1/f^2$  noise invokes the noise function six times more than the single noise function (yielding an expected value of 12 times). The  $1/f$ -noise rendering time was 27.5 times longer than that of single noise (less than the expected 36 times), and 3.75 times longer than the  $1/f^2$  noise (slightly larger than the expected value of 3).

## 5 Conclusion

Sphere tracing provides a tool for investigating a larger variety of implicit surfaces than before possible.

With its enhancements and prefiltering, sphere tracing becomes a competitive presentation-quality implicit surface renderer. In particular, the convexity enhancement greatly increases rendering speeds, and the triangle inequality is quite effective for large assortments of objects. Bounding volumes also increase rendering performance as expected. However, techniques based on image coherence and space coherence (octree) did not perform as well.

Whereas sphere tracing performed significantly slower than standard ray tracing on simple objects consisting of quadrics and polygons, it excelled at rendering the results of sophisticated geometric modeling operations.

The geometric nature of sphere tracing adapts it to symbolic prefiltering, supporting antialiasing at a nominal overhead.

In lieu of direct experimental comparison, several theoretical arguments show sphere tracing as a viable alternative to interval analysis and L-G surfaces.

### 5.1 Further Research

Sphere tracing demonstrates the utility of signed distance functions in the task of rendering geometric implicit surfaces. We expect these functions will similarly enhance other applications, particularly in the area of geometric processing. As geometric distance becomes more important in computer-aided geometric design and other areas of modeling, the demand for more efficient geometric distance algorithms will increase.

In retrospect, the use of the Euclidean distance metric seems an arbitrary choice for sphere tracing. The linear nature of the chessboard and Manhattan metrics may result in more efficiently computed distances and ray intersection. “Cube-tracing” and “octahedron-tracing” algorithms are left as further research.

## 5.2 Acknowledgements

Thanks to Tom DeFanti and Larry Smarr for their support of the first year of this research, and to Pat Flynn, Robert Bamberger and Tom Fischer for welcoming me and my research into the Imaging Research Laboratory at WSU.

This research is supported by the National Science Foundation under grant CCR-9309210. Any opinions, findings, conclusions or recommendations expressed in this manuscript are those of the author and do not necessarily reflect the view of the National Science Foundation.

Special thanks to Alan Norton who, in 1989, encouraged me to apply sphere tracing to non-fractal models. The task of tracking down and deriving the distances in the appendix was greatly helped by conversations with Al Barr, Chandrajit Bajaj, Charlie Gunn, Pat Hanrahan, Jim Kajiya, Don Mitchell and Alyn Rockwood.

Brian Wyvill and Jules Bloomenthal deserve special mention for inspiring this research by putting together an excellent course on implicit surfaces at SIGGRAPH '90.

## References

- [Agin & Binford, 1976] Agin, G. J. and Binford, T. O. Computer description of curved objects. *IEEE Transactions on Computers* C-25(4), Apr. 1976, pp. 439--449.
- [Amanatides, 1984] Amanatides, J. Ray tracing with cones. *Computer Graphics* 18(3), July 1984, pp. 129--135.
- [Ballard & Brown, 1982] Ballard, D. H. and Brown, C. M. *Computer Vision*. Prentice-Hall, Englewood Cliffs, NJ, 1982.

- [Barnhill *et al*, 1992] Barnhill, R. E., Frost, T. M., and Kersey, S. N. Self-intersections and offset surfaces. In Barnhill, R. E., ed., *Geometry Processing for Design and Manufacture*, pp. 35--44. SIAM, 1992.
- [Barr, 1981] Barr, A. H. Superquadrics and angle-preserving transformations. *IEEE Computer Graphics and Applications* 1(1), 1981, pp. 11--23.
- [Barr, 1984] Barr, A. H. Global and local deformations of solid primitives. *Computer Graphics* 18(3), July 1984, pp. 21--30.
- [Blinn, 1982] Blinn, J. F. A generalization of algebraic surface drawing. *ACM Transactions on Graphics* 1(3), July 1982, pp. 235--256.
- [Bloomenthal & Shoemake, 1991] Bloomenthal, J. and Shoemake, K. Convolution surfaces. *Computer Graphics* 25(4), July 1991, pp. 251--256.
- [Bloomenthal, 1988] Bloomenthal, J. Polygonization of implicit surfaces. *Computer Aided Geometric Design* 5(4), Nov. 1988, pp. 341--355.
- [Bloomenthal, 1989] Bloomenthal, J. Techniques for implicit modeling. Technical Report P89-00106, Xerox PARC, 1989. Appears in SIGGRAPH '93 Course Notes #25 "Design, Visualization and Animation of Implicit Surfaces".
- [Bronsvoort & Klok, 1985] Bronsvoort, W. F. and Klok, F. Ray tracing generalized cylinders. *ACM Transactions on Graphics* 4(4), Oct. 1985, pp. 291--303.
- [Farin, 1990] Farin, G. E. *Curves and Surfaces for Computer-Aided Geometric Design*. Academic Press, San Diego, 1990.
- [Gerald & Wheatley, 1989] Gerald, C. F. and Wheatley, P. O. *Applied Numerical Analysis*. Addison-Wesley, Reading, MA, 1989.
- [Goldman, 1983] Goldman, R. N. Two approaches to a computer model for quadric surfaces. *IEEE Computer Graphics and Applications* 3(5), Sept. 1983, pp. 21--24.

- [Hanrahan, 1983] Hanrahan, P. Ray tracing algebraic surfaces. *Computer Graphics* 17(3), 1983, pp. 83--90.
- [Hart & DeFanti, 1991] Hart, J. C. and DeFanti, T. A. Efficient antialiased rendering of 3-D linear fractals. *Computer Graphics* 25(3), 1991.
- [Hart *et al*, 1989] Hart, J. C., Sandin, D. J., and Kauffman, L. H. Ray tracing deterministic 3-D fractals. *Computer Graphics* 23(3), 1989, pp. 289--296.
- [Hart *et al*, 1993] Hart, J. C., Francis, G. K., and Kauffman, L. H. Visualizing quaternion rotation. Manuscript, in review, 1993.
- [Hart, 1994] Hart, J. C. Distance to an ellipsoid. In Heckbert, P., ed., *Graphics Gems IV*, pp. 113--119. Academic Press, 1994.
- [Hoffman, 1989] Hoffman, C. M. *Geometric and Solid Modeling*. Morgan Kaufmann, 1989.
- [Kalra & Barr, 1989] Kalra, D. and Barr, A. H. Guaranteed ray intersections with implicit surfaces. *Computer Graphics* 23(3), July 1989, pp. 297--306.
- [Kaplansky, 1977] Kaplansky, I. *Set Theory and Metric Spaces*. Chelsea, New York, 1977.
- [Kay & Kajiya, 1986] Kay, T. L. and Kajiya, J. T. Ray tracing complex scenes. *Computer Graphics* 20(4), 1986, pp. 269--278.
- [Lewis, 1989] Lewis, J. P. Algorithms for solid noise synthesis. *Computer Graphics* 23(3), July 1989, pp. 263--270.
- [Mitchell & Hanrahan, 1992] Mitchell, D. and Hanrahan, P. Illumination from curved reflectors. *Computer Graphics* 26(2), July 1992, pp. 283--291.
- [Mitchell, 1990a] Mitchell, D. P. The antialiasing problem in ray tracing. In *Advanced Topics in Ray Tracing*. SIGGRAPH '90 Course Notes, Aug. 1990.

- [Mitchell, 1990b] Mitchell, D. P. Robust ray intersection with interval arithmetic. In Proc. of *Graphics Interface '90*. Morgan Kaufman, 1990, pp. 68--74.
- [Nishimura *et al*, 1985] Nishimura, H., Hirai, M., Kawai, T., Kawata, T., Shirakawa, I., and Omura, K. Object modeling by distribution function and a method of image generation. In Proc. of *Electronics Communication Conference '85*, 1985, pp. 718--725. (Japanese).
- [Perlin & Hoffert, 1989] Perlin, K. and Hoffert, E. M. Hypertexture. *Computer Graphics* 23(3), July 1989, pp. 253--262.
- [Porter & Duff, 1984] Porter, T. and Duff, T. Compositing digital images. *Computer Graphics* 18(3), 1984, pp. 253--259.
- [Pratt, 1987] Pratt, V. Direct least-squares fitting of algebraic surfaces. *Computer Graphics* 21(4), July 1987, pp. 145--152.
- [Ricci, 1974] Ricci, A. A constructive geometry for computer graphics. *Computer Journal* 16(2), May 1974, pp. 157--160.
- [Rockwood & Owen, 1987] Rockwood, A. P. and Owen, J. C. Blending surfaces in solid modeling. In Farin, G., ed., *Geometric Modelling*, pp. 367--383. SIAM, 1987.
- [Rockwood, 1989] Rockwood, A. P. The displacement method for implicit blending surfaces in solid models. *ACM Transactions on Graphics* 8(4), Oct. 1989, pp. 279--297.
- [Roth, 1982] Roth, S. D. Ray casting for modeling solids. *Computer Graphics and Image Processing* 18(2), February 1982, pp. 109--144.
- [Sandin *et al*, 1993] Sandin, D. J., Kauffman, L. H., and Francis, G. K. Air on the Dirac strings. *SIGGRAPH Video Review* 93, 1993. (Animation).
- [Schneider, 1990] Schneider, P. J. Solving the nearest-point-on-curve problem. In Glassner, A. S., ed., *Graphics Gems (I)*, pp. 607--611. Academic Press, Boston, 1990.

- [Sederberg & Zundel, 1989] Sederberg, T. W. and Zundel, A. K. Scan line display of algebraic surfaces. *Computer Graphics* 23(3), July 1989, pp. 147--156.
- [Snyder, 1992] Snyder, J. M. Interval analysis for computer graphics. *Computer Graphics* 26(2), July 1992, pp. 121--130.
- [Stander & Hart, 1994] Stander, B. T. and Hart, J. C. A Lipschitz method for accelerated volume rendering. In Proc. of *Volume Visualization Symposium '94*, Oct. 1994. To appear.
- [Taubin, 1994] Taubin, G. Distance approximations for rasterizing implicit curves. *ACM Transactions on Graphics* 13(1), Jan. 1994, pp. 3--42.
- [Thomas *et al*, 1989] Thomas, D., Netravali, A. N., and Fox, D. S. Antialiased ray tracing with covers. *Computer Graphics Forum* 8(4), December 1989, pp. 325--336.
- [Thompson, 1990] Thompson, K. Area of intersection: Circle and a half-plane. In Glassner, A. S., ed., *Graphics Gems*, pp. 38--39. Academic Press, Boston, 1990.
- [van Wijk, 1984] van Wijk, J. Ray tracing objects defined by sweeping a sphere. In Proc. of *Eurographics '84*. Elsevier, 1984, pp. 73--82.
- [Von Herzen & Barr, 1987] Von Herzen, B. and Barr, A. H. Accurate triangulations of deformed, intersecting surfaces. *Computer Graphics* 21(4), July 1987, pp. 103--110.
- [Von Herzen *et al*, 1990] Von Herzen, B., Barr, A. H., and Zatz, H. R. Geometric collisions for time-dependent parameteric surfaces. *Computer Graphics* 24(4), Aug. 1990, pp. 39--48.
- [Voss, 1988] Voss, R. F. Fractals in nature: From characterization to simulation. In Peitgen, H. and Saupe, D., eds., *The Science of Fractal Images*, pp. 21--70. Springer-Verlag, New York, 1988.
- [Wyvill & Trotman, 1990] Wyvill, G. and Trotman, A. Ray tracing soft objects. In Proc. of *Computer Graphics International '90*. Springer Verlag, 1990.

[Wyvill *et al*, 1986] Wyvill, G., McPheeters, C., and Wyvill, B. Data structure for soft objects. *Visual Computer* 2(4), 1986, pp. 227--234.

[Zuiderveld *et al*, 1992] Zuiderveld, K. J., Koning, A. H. J., and Viergever, M. A. Acceleration of ray-casting using 3-D distance transforms. In Proc. of *Visualization in Biomedical Computing 1992*, vol. 1808, Oct. 1992, pp. 324--335.

## A Distance to Natural Quadrics and Torus

These appendices derive signed distance functions, bounds and Lipschitz constants and bounds for a variety of primitives and operations in the hope that they will aid in the implementation of sphere tracing, while also serving as a tutorial in developing signed distance functions, bounds and Lipschitz constants and bounds for other primitives and operations.

Distances to the standard solid modeling primitives are listed below. The geometric rendering algorithm is not as efficient compared to the standard closed-form solutions. Instead, these distances are useful when the primitives are used in higher-order constructions such as blends and deformations.

**Plane** The signed distance to a plane  $P$  with unit normal  $\mathbf{n}$  intersecting the point  $r\mathbf{n}$  is

$$d(\mathbf{x}, P) = \mathbf{x} \cdot \mathbf{n} - r. \quad (23)$$

**Sphere** A sphere is defined as the locus of points a fixed distance from given point. The distance to the unit sphere  $S$  about at the origin hence given by

$$d(\mathbf{x}, S) = \|\mathbf{x}\| - 1. \quad (24)$$

Through domain transformations (Section E, the radius and location of the sphere may be changed. The sphere may even become an ellipsoid, though this reformulates the signed distance function into one requiring the solution to a sixth-degree polynomial [Hart, 1994]. Through alternate distance metrics (Section B), the sphere can become a superellipsoid. These techniques also generalize the rest of the basic primitives as well.

**Cylinder** The distance to a unit-radius cylinder centered about the  $z$ -axis is found by projecting into the  $xy$ -plane and measuring the distance to the unit circle

$$d(\mathbf{x}, Cyl) = \|(x, y)\| - 1. \quad (25)$$

Note that in (25), and throughout the rest of the appendix,  $\mathbf{x} = (x, y, z)$ .

**Cone** The distance to a cone centered at the origin oriented along the  $z$ -axis is

$$d(\mathbf{x}, Cone) = \|(x, y)\| \cos \theta - |z| \sin \theta, \quad (26)$$

where  $\theta$  is the angle of divergence from the  $z$ -axis. The trigonometry behind its derivation is illustrated by Figure 14.

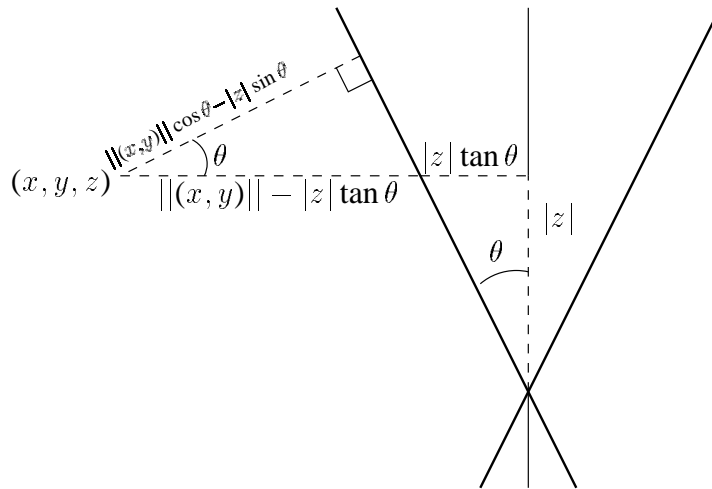


Figure 14: Geometry for distance to a cone.

**Torus** The torus is the product of two circles, and its distance is evaluated as such

$$d(\mathbf{x}, T) = \|(|(x, y)\| - R, z)\| - r \quad (27)$$

for a torus of major radius  $R$  and minor radius  $r$ , centered at the origin and spun about the  $z$ -axis.

## B Distance to Superquadrics

Superquadrics [Barr, 1981] result from the generalization of distance metrics. Distance to the basic primitives all used the  $\|\cdot\|$  operator. In two dimensions, this operator generalizes to the  $p$ -norm

$$\|(x, y)\|^p = (|x|^p + |y|^p)^{\frac{1}{p}} \quad (28)$$

which, when  $p = 2$ , becomes the familiar Euclidean metric whose *circle* is a round circle. The Manhattan metric ( $p = 1$ ) has a diamond for its *circle*. Taking the limit as  $p \rightarrow \infty$  results in the chessboard metric

$$\|(x, y)\|^\infty = \max x, y \quad (29)$$

where a square forms its *circle*. The other intervening values for  $p$  produce rounded variations on these basic shapes, and setting  $0 < p < 1$  produces pinched versions. Generalized spheres, so-called *superellipsoids*, are produced by a  $pq$ -norm as

$$\|(x, y, z)\|^{pq} = \|(\|(x, y)\|^p, z)\|^q. \quad (30)$$

The natural quadrics now generalize to superquadrics, and tori likewise become supertori, whose distances are measured in the appropriate metric. One unifying metric space must be used for the distances to be comparable. Hence,  $pq$ -norm distances must be converted into Euclidean distances.

Let  $f(\mathbf{x})$  return a  $pq$ -norm distance to its implicit surface. This distance defines the radius of an unbounding superellipsoid. The radius of the largest Euclidean sphere  $r_e$  inscribed within the  $pq$ -norm superellipsoid of radius  $r_s$  (in the  $pq$ -norm metric) is given by

$$r_e = \begin{cases} r_s / \|(\frac{\sqrt{3}}{3}, \frac{\sqrt{3}}{3}, \frac{\sqrt{3}}{3})\|^{pq} & \text{if } p < 2 \\ r_s & \text{otherwise} \end{cases} \quad (31)$$

## C Distance to Offset Surfaces

Given some closed skeleton geometry  $S \subset \mathbb{R}^3$ , then the *global* offset surface is defined geometrically by the implicit equation

$$d(\mathbf{x}, S) - r = 0. \quad (32)$$

When  $r$  is constant, the resulting implicit surface fleshes out the skeleton  $S$ .

The point-to-set distance is defined as a search through the entire set for the closest point. If  $\partial S$  has a surface normal defined everywhere, then the point  $\mathbf{y}$  in  $S$  closest to  $\mathbf{x}$  is one of the points on  $\partial S$  whose normal extends directly toward  $\mathbf{x}$ . This greatly reduces the search space for point-to-set distance determination to some primitives, such as parametric surfaces.

This formulation of the point-to-set distance can cause problems when used to define an offset, however. If the skeleton is a *generator* surface represented by the parametric function  $\mathbf{g}(u, v)$ , then the *local* offset surface is defined by the parametric function

$$\mathbf{p}(u, v) = \mathbf{g}(u, v) + r\mathbf{n}(u, v) \quad (33)$$

where

$$\mathbf{n}(u, v) = \frac{\mathbf{g}_u(u, v)}{\|\mathbf{g}_u(u, v)\|} \times \frac{\mathbf{g}_v(u, v)}{\|\mathbf{g}_v(u, v)\|} \quad (34)$$

is the unit-length surface normal at  $\mathbf{g}(u, v)$  and  $\mathbf{g}_u, \mathbf{g}_v$  are the partial derivatives with respect to  $u, v$ .

Global offsets are usually defined as geometric implicit surfaces whereas local offsets are usually defined parametrically. Global offsets are the more desirable representation [Hoffman, 1989], and in particular avoid interior surfaces which can cause problems in ray-tracing and CSG [van Wijk, 1984].

The offset of an algebraic implicit surface is algebraic, though of higher degree in general. Likewise, parametric versions of the offset surface are typically of higher degree than the generator. This increase in degree is due, in part, to the use of distance (requiring a cross product and square root in (34)) in the definition of offset surfaces. Several techniques have been developed to approximate offset surfaces with lower-degree representations. Treating offset surfaces geometrically overcomes the problems of dealing with unnecessarily high degree algebraic representations and loss of precision due to inexact low-degree approximations.

One useful skeletal model is the simplified generalized cylinder, which is a global offset surface defined as the locus of points a fixed distance from a space curve piecewise defined by 3-D Bezier curves.

Define the space curve parametrically as the image of the function  $\mathbf{p} : \mathbb{R} \rightarrow \mathbb{R}^3$ . Without loss of generality, assume the point we want to find the distance from the space curve is the origin.

Then the closest point on the space curve will be either of the endpoints, or a point on the space curve whose tangent is perpendicular with a vector pointing to the origin. The latter are found by solving

$$\mathbf{p}(u) \cdot \mathbf{p}_u(u) = 0. \quad (35)$$

Let  $\mathbf{p}$  be a cubic Bezier curve. Then [Schneider, 1990] shows how (35) can be converted into a degree-five 1-D Bezier curve, a Bernstein polynomial whose graph is bounded by the convex hull of the control points. Bernstein polynomials can be solved efficiently using a technique described in [Rockwood & Owen, 1987].

Generalized cylinders are demonstrated in Figure 9 in Section 4.2.

## D Distance to Blended Objects

A blend is a smoothing of the joint where sections of an object meet. The following two blends are local, meaning that they affect only a portion of the object. This is useful in computer-aided geometric design so that blends on different parts of an object do not interfere, and is useful in computer graphics to bound and cull blends from rendering when possible.

### D.1 Soft Metablobbies

[Blinn, 1982] used a Gaussian distribution function to produce a blending function which has come to be known as the ‘‘blobby’’ model. ‘‘Soft’’ objects approximate Gaussian distribution with a sixth-degree polynomial to avoid exponentiation and localize the blends [Wyvill *et al*, 1986]. ‘‘Metaballs’’ approximate Gaussian distributions with piecewise quadratics to avoid exponentiation and iterative root-finding [Nishimura *et al*, 1985].

Following [Wyvill *et al*, 1986], the following piecewise cubic in distance  $r$

$$C_R(r) = \begin{cases} 2\frac{r^3}{R^3} - 3\frac{r^2}{R^2} + 1 & \text{if } r < R, \\ 0 & \text{otherwise.} \end{cases} \quad (36)$$

approximates a Gaussian distribution. A similar sixth-degree algebraic version also exists and is typically used instead, avoiding distance computations at the expense of the higher degree [Wyvill & Trotman, 1990].

Reformulating this function to accommodate the implicit surface definitions in this paper, (36) forms the basis for a *soft* implicit surface consisting of  $n$  key points  $\mathbf{p}_i$  with radii  $R_i$ , and threshold  $T$ , defined by the function

$$f(\mathbf{x}) = T - \sum_{i=1}^n C_{R_i}(\|\mathbf{x} - \mathbf{p}_i\|) \quad (37)$$

Negative keypoints are incorporated into the model by negating the value returned by  $C_{R_i}()$ .

**Theorem 5** *The distance to the implicit blend  $B$  defined by (37) is bounded by*

$$d(\mathbf{x}, B) \geq \frac{2}{3} f(\mathbf{x}) \sum_{i=1}^n R_i. \quad (38)$$

**Proof:** Repeated differentiation of (36) produces

$$C'(r) = 6 \frac{r^2}{R^3} - 6 \frac{r}{R^2} \quad (39)$$

$$C''(r) = 12 \frac{r}{R^3} - \frac{6}{R^2}. \quad (40)$$

Solving  $C''(r) = 0$  yields the maximum slope, which occurs at the midpoint  $r = R/2$ . Its Lipschitz constant is given by

$$\text{Lip } C(r) = |C'(R/2)| = \frac{3}{2R}. \quad (41)$$

The Lipschitz constant of a sum is bounded by the sum of the Lipschitz constants, which gives the above result.  $\square$

In practice, local Lipschitz bounds may be used for tighter distance bounds by taking the first summation in (38) over keypoints  $i$  with non-zero contributions. Additional efficiency results from the use of bounding volumes of radius  $R_i$  surrounding the keypoints  $\mathbf{p}_i$ , as detailed in [Wyvill & Trotman, 1990].

## D.2 Superelliptic Blends

The pseudonorm blend of [Rockwood & Owen, 1987] is a local blend. It returns the  $p$ -norm distance to the blended union of implicit surfaces of signed distance functions. This blend is based

on the pioneering work of [Ricci, 1974], where implicit surfaces were defined by setting strictly non-negative functions equal to one. Hence, we need to reformulate our functions into this style by defining

$$g_A(\mathbf{x}) = \max\left\{1 - \frac{f_A(\mathbf{x})}{r_A}, 0\right\} \quad (42)$$

and similarly for  $g_B$ . The parameters  $r_A, r_B$  will delineate the extent of the local blends, in Euclidean units if the components are signed distance functions. The pseudonorm blend of the union of the implicit surface of  $f_A$  with the implicit surface of  $f_B$  is defined by the implicit surface of

$$f_{AB}(f_A(\mathbf{x}), f_B(\mathbf{x})) = \left( \frac{g_A(\mathbf{x})r_A + g_B(\mathbf{x})r_B}{g_A(\mathbf{x}) + g_B(\mathbf{x})} (1 - g_A(\mathbf{x})^p - g_B(\mathbf{x})^p) \right)^{\frac{1}{p}}. \quad (43)$$

The parameter  $p$  is a *thumbweight* which describes how tightly the blend adheres to the original surfaces. Conversely, the blended intersection is defined by  $-f_{AB}(-f_A(\mathbf{x}), -f_B(\mathbf{x}))$ .

The domain of  $f_{AB}$  is the area where  $f_A(\mathbf{x}) \leq r_A$  and  $f_B(\mathbf{x}) \leq r_B$ . Outside this domain, it is impossible to smoothly combine the results of  $f_A$  and  $f_B$ , resulting in a crease in the space surrounding the blend [Rockwood & Owen, 1987]. Such gradient discontinuities can be disastrous for some root finders, but do not impact the geometric ray intersection method described earlier.

The pseudonorm blend is demonstrated in Figures 8 and 10 in Section 4.2.

## E Distances to Transformed Objects

Implicit surfaces are transformed by applying the inverse transformation to the space before applying the function. Let  $T(\mathbf{x})$  be a transformation and let  $f(\mathbf{x})$  define the implicit surface. Then the transformed implicit surface is defined as the implicit surface of

$$f(T^{-1}(\mathbf{x})) = 0. \quad (44)$$

The Lipschitz constant of the composition is no greater than the product of the component Lipschitz constants. We are concerned with the Lipschitz constant of the transformation inverse, which is not necessarily the inverse of the Lipschitz constant of the transformation.

**Isometry** Isometries are transformations that preserve distances. If  $I$  is an isometry, the distance returned by  $f$  needs no adjustment

$$d(\mathbf{x}, I \circ f^{-1}(0)) = d(I^{-1}(\mathbf{x}), f^{-1}(0)). \quad (45)$$

Isometries include rotations, translations and reflections.

**Uniform Scale** A uniform scale is a transformation  $S(\mathbf{x})$  of the form

$$S(\mathbf{x}) = s\mathbf{x} \quad (46)$$

where  $s$  is the scale factor. The inverse  $S^{-1}$  is a scale by  $1/s$ . Hence, the distance to a scaled implicit surface is

$$d(\mathbf{x}, S(f^{-1}(0))) = sd(S^{-1}(\mathbf{x}), f^{-1}(0)) \quad (47)$$

and the Lipschitz constant of the inverse scale is  $1/s$ .

**Linear Deformation** The distance to the linear image of an implicit surface is found by determining the Lipschitz constant of the linear transformation's inverse, which is also a linear transformation.

The Lipschitz constant of an arbitrary linear transformation is found by the power method, which iteratively finds the largest eigenvalue of a matrix [Gerald & Wheatley, 1989].

**Taper** The taper deformation scales two axes by a function  $r(\cdot)$  of the third axis [Barr, 1984]. The taper is defined

$$\text{taper}(\mathbf{x}) = (r(z)x, r(z)y, z) \quad (48)$$

whereas its inverse differs only by using  $r^{-1}(\cdot)$  instead of  $r(\cdot)$ . The Lipschitz constant of the inverse deformation is

$$\text{Lip taper} = \min_{z \in \mathbb{R}} r^{-1}(z). \quad (49)$$

In other words, the Lipschitz constant of the inverse taper is the amount of its ‘‘tightest’’ tapering.

**Twist** The twisting deformation rotates two axes by a linear function  $a(\cdot)$  of the third axis. Twisting is defined

$$\text{twist}(\mathbf{x}) = \begin{pmatrix} x \cos a(z) - y \sin a(z), \\ x \sin a(z) + y \cos a(z), \\ z \end{pmatrix} \quad (50)$$

whereas its inverse differs only by using  $a^{-1}(\cdot)$  instead of  $a(\cdot)$ . Twisting is not Lipschitz on  $\mathbb{R}^n$  since for any Lipschitz bound  $\lambda$  one can find two points  $\mathbb{R}^n$  at a great distance from the twisting axis that are transformed farther apart by a ratio greater than  $\lambda$ . Thus, twisting must be constrained to a domain where it satisfies the Lipschitz criterion. One such domain is the unit cylinder oriented along the twisting axis. The Lipschitz constant of the twist is computed from the worst case scenario within the bounds of the unit cylinder as illustrated in Figure 15,

$$\text{Lip twist} = \sqrt{4 + \left(\frac{\pi}{a'}\right)^2}. \quad (51)$$

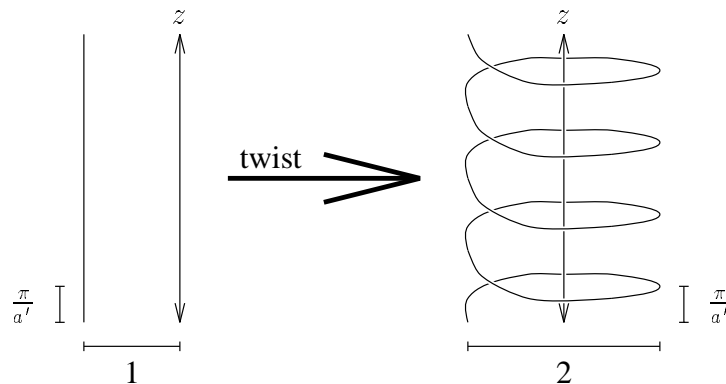


Figure 15: Geometric calculation of the Lipschitz constant of the bounded twist deformation.

## F Distance to Hypertextures

The use of sophisticated noise functions has greatly increased the power of procedural models for making existing geometric representations more realistic. The recent work has applied stochastic

textures directly to the geometry instead of altering the shading [Perlin & Hoffert, 1989; Lewis, 1989].

The original ‘‘Hypertexture’’ system formulated implicit models for a variety of surface phenomena, including hair and fire. This appendix focuses on incorporating hypertexture’s model of noise into sphere tracing, though the same techniques can be used to adapt the other hypertexture models as well.

‘‘Hypertexture’’ treats solid procedural noise as a deformation, and was designed for use with implicit surfaces. Its original ray-tracing algorithm stepped along the ray in fixed intervals. Determining a distance bound on a ‘‘hypertextured’’ shape allows sphere tracing to more efficiently render its result.

Departing slightly from [Perlin & Hoffert, 1989], a noise function  $\text{noise} : \mathbb{R}^3 \rightarrow \mathbb{R}$  deforms the implicit surface of a signed distance function  $f$  by affecting its range (instead of its domain, as did the previous appendix). The deformed surface is defined implicitly by the function  $f(\mathbf{x}) + \text{noise}(\mathbf{x})$ .

Band-limited solid noise results from the smooth interpolation of a lattice of random unit vectors. Condensing [Perlin & Hoffert, 1989], the noise function is given by

$$\text{noise}(x, y, z) = \sum_{k=\lfloor z \rfloor}^{\lfloor z \rfloor + 1} \sum_{j=\lfloor y \rfloor}^{\lfloor y \rfloor + 1} \sum_{i=\lfloor x \rfloor}^{\lfloor x \rfloor + 1} C_1(|x - i|)C_1(|y - j|)C_1(|z - k|)\Gamma(i, j, k) \cdot (x - i, y - j, z - k) \quad (52)$$

where  $C_R$  is the cubic Gaussian approximation (36) used for soft objects, and  $\Gamma$  is an array of random unit vectors. From Theorem 5, we know that  $\text{Lip } C_1 = 3/2$ . Two opposing vectors can be neighbors in  $\Gamma$ , so  $\text{Lip } \Gamma = 2$ . Hence, their composition results in  $\text{Lip noise} = 3$ .

Fractal noise based on the  $1/f^\beta$  spectral distribution are formed by summing scaled versions of the noise function

$$1/f^\beta \text{ noise}(\mathbf{x}) = \sum_{i=0}^{n-1} \frac{\text{noise}(2^i \mathbf{x})}{2^{\beta i}}. \quad (53)$$

over  $n$  octaves [Perlin & Hoffert, 1989].

Setting the parameter  $\beta = 0$  results in white noise,  $\beta = 1$  in  $1/f$  noise typically found in nature and  $\beta = 2$  in Brownian motion. When in the range  $1 \leq \beta \leq 3$ , its relationship to the fractal dimension  $D$  of the resulting surface it deforms is given by  $D = 2 + \frac{3-\beta}{2}$  [Voss, 1988]. The  $2^i$  factor increases the frequency (contracts the graph horizontally) whereas the  $1/2^{\beta i}$  factor decreases the

amplitude (contracts the graph vertically).

For  $1/f$  noise, the amplitude decreases proportionately to the increase in frequency, so its Lipschitz constant equals the sum of the individual noise functions,

$$\text{Lip } 1/f \text{ noise} = 3n. \quad (54)$$

Thus  $1/f$  noise is not Lipschitz, but its band-limited form for finite  $n$  is.

For Brownian motion ( $\beta = 2$ ), the amplitude decreases geometrically as the frequency increases, resulting in

$$\text{Lip } 1/f^2 \text{ noise} = 3(2 - 1/2^{n-1}) \leq 6. \quad (55)$$

Hence, Brownian motion is Lipschitz (which can also be derived from the definition of Brownian motion as the integral of white noise).

The noise functions are demonstrated in Figure 11 in Section 4.2.